

Hardware and Interference Limited Cooperative CR-NOMA Networks under Imperfect SIC and CSI

Sultangali Arzykulov, *Member, IEEE*, Galymzhan Nauryzbayev, *Member, IEEE*,
Abdulkadir Celik, *Senior Member, IEEE*, and Ahmed M. Eltawil, *Senior Member, IEEE*

Abstract—The conflation of cognitive radio (CR) and non-orthogonal multiple access (NOMA) concepts is a promising approach to fulfill the massive connectivity goals of future networks given the spectrum scarcity. Accordingly, this letter investigates the outage performance of imperfect cooperative CR-NOMA networks under hardware impairments and interference. Our analysis is involved with the derivation of the end-to-end outage probability (OP) for secondary NOMA users by accounting for imperfect channel state information (CSI), as well as the residual interference caused by successive interference cancellation (SIC) errors and coexisting primary/secondary users. The numerical results validated by Monte Carlo simulations show that CR-NOMA network provides a superior outage performance over orthogonal multiple access. As imperfections become more significant, CR-NOMA is observed to deliver relatively poor outage performance.

Index Terms—Cognitive radio, cooperative non-orthogonal multiple access, outage probability, hardware impairment.

I. INTRODUCTION

THE ambitious quality-of-service (QoS) demands of future wireless networks poses daunting challenges, especially under the ever-increasing number of devices connected to the Internet [1]. This consequently leads to two problems: spectrum scarcity and interference-limited networks. Spectrum scarcity has been mostly studied in the realm of cognitive radio (CR) networks where unlicensed/secondary users are permitted to operate on spectrum bands licensed to primary users in an opportunistic and non-intrusive manner [2]. Alternatively, non-orthogonal multiple access (NOMA) schemes have also recently received attention as a promising technique to mitigate the inability of orthogonal multiple access (OMA) schemes to support massive connectivity [3]. On the transmitter side, the NOMA scheme superposes messages of intended users with distinctive power allocation (PA) weights based on their channel quality. On the receiver side, the intended signal is extracted by decoding the transmitted broadcast message using successive interference cancellation (SIC).

Therefore, the conflation of CR and NOMA concepts (CR-NOMA) is regarded as a potential solution to the problems mentioned above. Existing literature on cooperative CR-NOMA networks mostly deals with simple scenarios under ideal cases without paying sufficient attention to practical limitations in terms of channel and hardware impairments [4]–[7]. Accordingly, this letter investigates the outage performance of a generic and imperfect CR-NOMA, where non-ideality is modeled by accounting for hardware impairments (HIs), channel state information (CSI) imperfections, and residual interference due to the SIC error propagation. Ensuring that

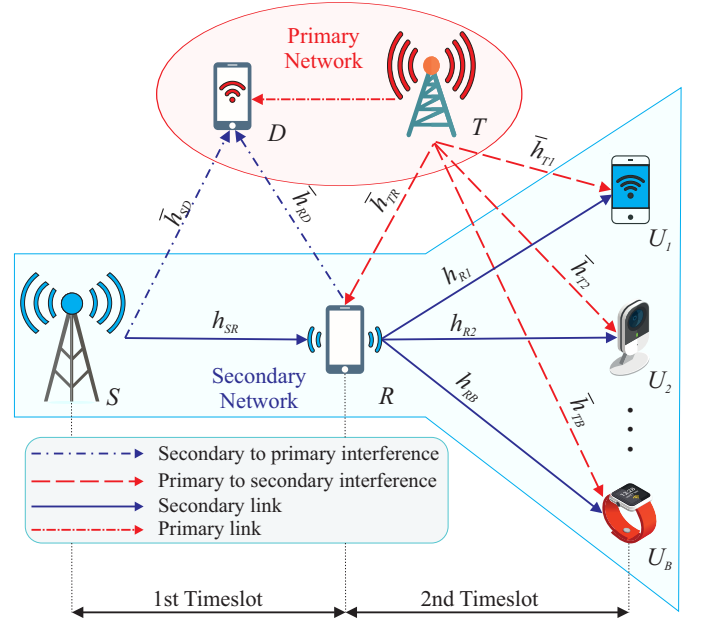


Fig. 1. The proposed underlay CR-NOMA network.

primary traffic is protected, our analysis also tackles the random interference caused by coexisting primary/secondary users. The numerical results validated by Monte Carlo simulations show that the CR-NOMA network provides a superior outage performance over orthogonal multiple access, which degrades with CSI and SIC imperfections.

II. SYSTEM MODEL

A. Channel Model

We consider a downlink CR-NOMA network that consists of primary and secondary networks as illustrated in Fig. 1. The primary network comprises of primary transmitter (T) and destination (D) nodes. On the other hand, the secondary network consists of a source (S), a relay (R) that cooperates with S in a half-duplex decode-and-forward (DF) mode, and B secondary NOMA users. The cooperation occurs in two time slots; The broadcast signal transmitted by S in the first time slot is re-transmitted to B NOMA users in the second time slot. Channel gains among the nodes are modeled as $\bar{h}_i \sim \mathcal{CN}(0, 1)$, $\forall i \in \{SD, SR, RD, R1, \dots, RB, TR, T1, \dots, TB\}$. Moreover, the distance between the corresponding nodes and the path-loss exponent are denoted by d_i and τ , respectively. To capture

CSI imperfections, we model channel coefficients using the minimum mean square error (MMSE) channel estimator as $\bar{h}_i = h_i + e_i$, where $h_i \sim \mathcal{CN}(0, \sigma_{h_i}^2)$ and $e_i \sim \mathcal{CN}(0, \zeta_i)$ are the estimated channel coefficient and channel estimation error with variance $\sigma_{h_i}^2$ and ζ_i , respectively. The error variance is modeled as $\zeta_i \triangleq \theta \rho^{-\kappa}$ where $\rho = \frac{P}{\sigma^2}$ is the transmitted signal-to-noise ratio (SNR), and $\kappa \geq 0$, $\theta > 0$ [8]. Indeed, this model describes various CSI acquisition scenarios: a) ζ is a function of ρ for $\kappa \neq 0$, and b) ζ is independent of ρ for $\kappa = 0$. Following from the underlay CR paradigm, it is also assumed that the transmit power of a secondary node $j \in \{R, S\}$ is restricted as [9] $P_j \leq \min\left(\bar{P}_j, \frac{I_{\text{ITC},j}}{|h_{jD}|^2}\right)$, where \bar{P}_j stands for the maximum transmit power at node j and $I_{\text{ITC},j}$ denotes the interference temperature constraint (ITC) at D caused by node j .

B. Transmission Protocol

In the first time slot of the proposed CR-NOMA relaying model, S broadcasts $\sum_{b=1}^B \sqrt{\alpha_b} x_b$ to R , where α_b is the PA factor¹ of U_b such that $\alpha_1 > \dots > \alpha_b > \dots > \alpha_B$ and $\sum_{b=1}^B \alpha_b = 1$, and x_b is the message dedicated to U_b with $\mathbb{E}(|x_b|^2) = 1$.

Considering CSI imperfections and aggregate distortion noise, the received signal at R can be written as

$$y_R = (h_{SR} + e_{SR}) \sqrt{\tilde{P}_S} \left(\sum_{b=1}^B \sqrt{\alpha_b} x_b + \eta_{SR} \right) + \bar{h}_{TR} \sqrt{\tilde{P}_T} (x_T + \eta_T) + n_R, \quad (1)$$

where $\tilde{P}_i = \frac{P_i}{d_{iR}^2}$, $i \in \{S, T\}$; $\eta_{(\cdot)} \sim \mathcal{CN}(0, \phi_{(\cdot)}^2)$ denotes the aggregate distortion noise from transceiver; $\phi_{(\cdot)} = \sqrt{\phi_t^2 + \phi_r^2}$ is the aggregate HI level from the transmitter and receiver [11]; $n_{(\cdot)} \sim \mathcal{CN}(0, \sigma_{(\cdot)}^2)$ denotes the additive white Gaussian noise (AWGN) term at each receiver node; P_T and x_T stand for the transmit power at T and the message dedicated to D , respectively. Then, the instantaneous signal-to-interference-distortion-noise-ratio (SIDNR) to decode x_j , $1 \leq j \leq b < B$, at R can be expressed by

$$\gamma_{R,j} = \frac{\alpha_j P_S |h_{SR}|^2}{\mathcal{A} P_S |h_{SR}|^2 + \mathcal{C} P_S + \mathcal{D}_R \tilde{P}_T |\bar{h}_{TR}|^2 + d_{SR}^{\tau} \sigma_R^2}, \quad (2)$$

where $\mathcal{A} = \Omega_j + \tilde{\Omega}_j + \phi_{SR}^2$; $\Omega_j = \sum_{n=j+1}^B \alpha_n$; $\tilde{\Omega}_j = \sum_{\tilde{n}=1}^{j-1} \vartheta_{\tilde{n}} \alpha_{\tilde{n}}$, $0 < \vartheta_{\tilde{n}} < 1$, where $\vartheta_{\tilde{n}} = 0$ and $\vartheta_{\tilde{n}} = 1$ indicate the perfection and absence of SIC, respectively; $\mathcal{C} = \zeta_{SR} + \zeta_{SR} \phi_{SR}^2$ and $\mathcal{D}_R = d_{SR}^{\tau} d_{TR}^{\tau} (1 + \phi_{TR}^2)$. Furthermore, by assuming imperfect detection of x_j , R decodes the message of user B with the SIDNR of

$$\gamma_{R,B} = \frac{\alpha_B P_S |h_{SR}|^2}{\tilde{\mathcal{A}} P_S |h_{SR}|^2 + \mathcal{C} P_S + \mathcal{D}_R \tilde{P}_T |\bar{h}_{TR}|^2 + d_{SR}^{\tau} \sigma_R^2}, \quad (3)$$

where $\tilde{\mathcal{A}} = (\tilde{\Omega}_B + \phi_{SR}^2)$ and $\tilde{\Omega}_B = \sum_{\tilde{n}=1}^{B-1} \vartheta_{\tilde{n}} \alpha_{\tilde{n}}$.

In the second time slot, R relays the decoded signal $\sum_{b=1}^B \sqrt{\beta_b} \tilde{x}_b$ to B NOMA users, where β_b , with $\sum_{b=1}^B \beta_b = 1$, is the PA factor of U_b . Hence, the received signal at U_b can be written as

$$y_b = (h_{Rb} + e_b) \sqrt{\tilde{P}_R} \left(\sum_{j=1}^B \sqrt{\beta_j} x_j + \eta_b \right) + \bar{h}_{Tb} \sqrt{\tilde{P}_T} (x_T + \eta_T) + n_b, \quad (4)$$

where $\tilde{P}_i = \frac{P_i}{d_{ib}^2}$, $i \in \{R, T\}$. Then, we can write the SIDNR for U_b to detect the message of U_j as follows

$$\gamma_{b,j} = \frac{\beta_j P_R |h_{Rb}|^2}{\mathcal{J}_b P_R |h_{Rb}|^2 + \mathcal{G}_b P_R + \mathcal{D}_b \tilde{P}_T |\bar{h}_{Tb}|^2 + d_{Rb}^{\tau} \sigma_b^2}, \quad (5)$$

where $\beta_1 > \beta_j > \beta_b > \beta_B$; $\forall b \in \{1, \dots, B\}$; $\mathcal{J}_b = (\Omega_j + \tilde{\Omega}_j + \phi_b^2)$; $\Omega_j = \sum_{n=j+1}^B \beta_n$; $\tilde{\Omega}_j = \sum_{\tilde{n}=1}^{j-1} \vartheta_{\tilde{n}} \beta_{\tilde{n}}$; $\mathcal{G}_b = (\zeta_b + \zeta_b \phi_b^2)$ and $\mathcal{D}_b = d_{Rb}^{\tau} d_{Tb}^{\tau} (1 + \phi_{Tb}^2)$. Finally, after decoding messages of $B-1$ NOMA users, U_B detects its own message with

$$\gamma_B = \frac{\beta_B P_R |h_{RB}|^2}{\mathcal{J}_B P_R |h_{RB}|^2 + \mathcal{G}_B P_R + \mathcal{D}_B \tilde{P}_T |\bar{h}_{TB}|^2 + d_{RB}^{\tau} \sigma_B^2}, \quad (6)$$

where $\mathcal{J}_B = \tilde{\Omega}_B + \phi_B^2$; $\tilde{\Omega}_B = \sum_{\tilde{n}=1}^{B-1} \vartheta_{\tilde{n}} \beta_{\tilde{n}}$. Considering the dual-hop communication, the achievable rate at U_j is calculated as

$$\mathcal{R}_j = \frac{1}{2} \log_2 [1 + \min(\gamma_{R,j}, \gamma_{b,j})], \quad 1 \leq j \leq b \leq B. \quad (7)$$

III. OUTAGE ANALYSIS

The outage at U_j occurs when the achievable rate at U_j is below a predefined rate threshold $\mathcal{R}_{\text{th},j}$. Following from (7), the OP of U_j can be written as

$$\begin{aligned} P_{\text{out},j} &= \Pr \left[\frac{1}{2} \log_2 [1 + \min(\gamma_{R,j}, \gamma_{b,j})] < \mathcal{R}_{\text{th},j} \right] \\ &= 1 - \Pr [\min(\gamma_{R,j}, \gamma_{b,j}) > \psi_j] \\ &= F_{\gamma_{R,j}}(\psi_j) + F_{\gamma_j}(\psi_j) - F_{\gamma_{R,j}}(\psi_j) F_{\gamma_j}(\psi_j), \end{aligned} \quad (8)$$

where $\psi_j = 2^{2\mathcal{R}_{\text{th},j}} - 1$ denotes the predefined SNR threshold at U_j . Now, considering the ITC imposed at D , we can write the CDF of the RV $\gamma_{R,j}$ as in (9), where $X = |h_{SR}|^2$, $Y = |\bar{h}_{SD}|^2$ and $Z = |\bar{h}_{PR}|^2$ follow the exponential distribution with parameter λ ; $\mathcal{K}_c = \frac{\mathcal{D}_R \tilde{P}_T \psi_j}{d(\alpha_j - \mathcal{A} \psi_j)}$; $\mathcal{M}_c = \frac{\psi_j d_{SR}^{\tau} \sigma_j^2}{d(\alpha_j - \mathcal{A} \psi_j)}$, with $c = d$, $c \in \{\Delta, \Upsilon\}$ and $d \in \{\bar{P}_S, I_{\text{ITC}} d_{SD}^{\tau}\}$; $\mathcal{L} = \frac{\mathcal{C} \psi_j}{\alpha_j - \mathcal{A} \psi_j}$ and $\Lambda_S = \frac{I_{\text{ITC}} d_{SD}^{\tau}}{P_S}$.

Proposition 1: The CDF of $\gamma_{R,j}$ can be derived in its closed-form as

$$\begin{aligned} F_{\gamma_{R,j}}(\psi_j) &= 1 - \frac{\lambda_z e^{-\lambda_x (\mathcal{M}_\Delta + \mathcal{L})}}{\lambda_z + \lambda_x \mathcal{K}_\Delta} (1 - e^{-\lambda_y \Lambda_S}) \\ &\quad + \frac{\lambda_y \lambda_z \text{Ei}[-\mu_S \xi_S]}{\lambda_x \mathcal{K}_\Upsilon} e^{-\Lambda_S (\lambda_y + \lambda_x \mathcal{M}_\Upsilon) - \lambda_x \mathcal{L} + \mu_S \xi_S}. \end{aligned} \quad (10)$$

Proof: See Appendix A. ■

¹Similar to [10], we allocate the power based on the QoS requirements imposed at secondary NOMA users.

$$\begin{aligned}
F_{\gamma_{R,j}}(\psi_j) &= \Pr \left[\frac{\alpha_j \bar{P}_S |h_{SR}|^2}{A \bar{P}_S |h_{SR}|^2 + C \bar{P}_S + \mathcal{D}_R \tilde{P}_T |\bar{h}_{TR}|^2 + d_{SR}^2 \sigma_R^2} < \psi_j, \bar{P}_S < \frac{I_{\text{ITC}} d_{SD}^2}{|\bar{h}_{SD}|^2} \right] \\
&+ \Pr \left[\frac{\frac{\alpha_j I_{\text{ITC}} d_{SD}^2 |h_{SR}|^2}{|\bar{h}_{SD}|^2}}{\frac{A I_{\text{ITC}} d_{SD}^2 |h_{SR}|^2}{|\bar{h}_{SD}|^2} + \frac{C I_{\text{ITC}} d_{SD}^2}{|\bar{h}_{SD}|^2} + \mathcal{D}_R \tilde{P}_T |\bar{h}_{TR}|^2 + d_{SR}^2 \sigma_R^2} < \psi_j, \bar{P}_S > \frac{I_{\text{ITC}} d_{SD}^2}{|\bar{h}_{SD}|^2} \right] \\
&= \underbrace{\Pr[X < ZK_\Delta + \mathcal{M}_\Delta + \mathcal{L}, Y < \Lambda_S]}_{\Delta} + \underbrace{\Pr[X < ZYK_\Upsilon + Y\mathcal{M}_\Upsilon + \mathcal{L}, Y > \Lambda_S]}_{\Upsilon}, \quad (9)
\end{aligned}$$

Following from (5), the CDF of $\gamma_{b,j}$ can be described as

$$\begin{aligned}
F_{\gamma_{b,j}}(\psi_j) &= \underbrace{\Pr[Q < WS_\Theta + \mathcal{O}_\Theta + \mathcal{T}, V < \Lambda_R]}_{\Theta} \\
&+ \underbrace{\Pr[Q < WV\mathcal{S}_\Phi + V\mathcal{O}_\Phi + \mathcal{T}, V > \Lambda_R]}_{\Phi}, \quad (11)
\end{aligned}$$

where $Q = |h_{RB}|^2$; $V = |\bar{h}_{RD}|^2$; $W = |\bar{h}_{TB}|^2$; $\mathcal{S}_k = \frac{\mathcal{D}_b \tilde{P}_T \psi_j}{l(\beta_b - \mathcal{J}_b \psi_j)}$; $\mathcal{O}_k = \frac{d_{RB}^2 \sigma_k^2 \psi_j}{l(\beta_b - \mathcal{J}_b \psi_j)}$, with $k = l, k \in \{\Theta, \Phi\}$ and $l \in \{\bar{P}_R, I_{\text{ITC}} d_{RD}^2\}$; $\mathcal{T} = \frac{\mathcal{G}_b \psi_j}{\beta_b - \mathcal{J}_b \psi_j}$ and $\Lambda_R = \frac{I_{\text{ITC}} d_{RD}^2}{\bar{P}_R}$.

Proposition 2: The closed-form expression for the CDF of $\gamma_{b,j}$ can be written as

$$\begin{aligned}
F_{\gamma_{b,j}}(\psi_j) &= 1 - \frac{\lambda_w e^{-\lambda_q(\mathcal{O}_\Theta + \mathcal{T})}}{\lambda_w + \lambda_q \mathcal{S}_\Theta} (1 - e^{-\lambda_v \Lambda_R}) \\
&+ \frac{\lambda_v \lambda_w \text{Ei}[-\mu_R \xi_R]}{\lambda_q \mathcal{S}_\Phi} e^{-\Lambda_R(\lambda_v + \lambda_q \mathcal{O}_\Phi) - \lambda_q \mathcal{T} + \mu_R \xi_R}. \quad (12)
\end{aligned}$$

Proof: See Appendix B. ■

Lastly, the exact OP of U_j can be derived after substituting (10) and (12) into (8). Similarly, the OP of the U_M can be derived by using (2) and (6) and following the same procedure in obtaining the OP of U_j . Then, following the similar approach as in Appendix A, the CDFs of the RV $\gamma_{R,B}$ can be derived in closed-form as

$$\begin{aligned}
F_{\gamma_{R,B}}(\psi_B) &= 1 - \frac{\lambda_z e^{-\lambda_x(\mathcal{H}_\Psi + \mathcal{I})}}{\lambda_z + \lambda_x \mathcal{E}_\Psi} (1 - e^{-\lambda_y \Lambda_S}) \\
&+ \frac{\lambda_y \lambda_z \text{Ei}[-\bar{\mu}_S \bar{\xi}_S]}{\lambda_x \mathcal{E}_\Pi} e^{-\Lambda_S(\lambda_y + \lambda_x \mathcal{H}_\Pi) - \lambda_x \mathcal{I} + \bar{\mu}_S \bar{\xi}_S}, \quad (13)
\end{aligned}$$

where $\mathcal{E}_m = \frac{\mathcal{D}_R \tilde{P}_T \psi_B}{d(\alpha_B - \bar{\mathcal{A}} \psi_B)}$; $\mathcal{H}_m = \frac{d_{RB}^2 \sigma_B^2 \psi_B}{d(\alpha_B - \bar{\mathcal{A}} \psi_B)}$, with $m = d$, $m \in \{\Psi, \Pi\}$ and $d \in \{\bar{P}_S, I_{\text{ITC}} d_{SD}^2\}$; $\mathcal{I} = \frac{\mathcal{C} \psi_B}{\alpha_B - \bar{\mathcal{A}} \psi_j}$; $\bar{\mu}_S = \lambda_z + \lambda_x \Lambda_S \mathcal{E}_\Pi$; $\bar{\xi}_S = \frac{\mathcal{H}_\Pi}{\mathcal{E}_\Pi} + \frac{\lambda_y}{\lambda_x \mathcal{E}_\Pi}$. Moreover, $\psi_B < \frac{\alpha_B}{\bar{\mathcal{A}}}$, otherwise, $F_{\gamma_{R,B}}(\psi_B) \sim 1$. Similarly, the CDF of γ_B is derived as

$$\begin{aligned}
F_{\gamma_B}(\psi_B) &= 1 - \frac{\lambda_{\bar{w}} e^{-\lambda_{\bar{q}}(\bar{\mathcal{O}}_\Xi + \bar{\mathcal{T}})}}{\lambda_{\bar{w}} + \lambda_{\bar{q}} \bar{\mathcal{S}}_\Xi} (1 - e^{-\lambda_{\bar{v}} \Lambda_R}) \\
&+ \frac{\lambda_{\bar{v}} \lambda_{\bar{w}} \text{Ei}[-\bar{\mu}_R \bar{\xi}_R]}{\lambda_{\bar{q}} \bar{\mathcal{S}}_\aleph} e^{-\Lambda_R(\lambda_{\bar{v}} + \lambda_{\bar{q}} \bar{\mathcal{O}}_\aleph) - \lambda_{\bar{q}} \bar{\mathcal{T}} + \bar{\mu}_R \bar{\xi}_R}, \quad (14)
\end{aligned}$$

where $\bar{\mathcal{Q}} = |h_{RB}|^2$; $\bar{W} = |\bar{h}_{TB}|^2$; $\bar{\mathcal{S}}_r = \frac{\bar{\mathcal{D}}_B \tilde{P}_T \psi_B}{n(\beta_B - \bar{\mathcal{J}}_B \psi_B)}$; $\bar{\mathcal{O}}_r = \frac{d_{RB}^2 \sigma_B^2 \psi_B}{n(\beta_B - \bar{\mathcal{J}}_B \psi_B)}$, with $r = n$, $r \in \{\Xi, \aleph\}$ and $n \in \{\bar{P}_R, I_{\text{ITC}} d_{RD}^2\}$; $\bar{\mathcal{T}} = \frac{\bar{\mathcal{G}}_B \psi_B}{\beta_B - \bar{\mathcal{J}}_B \psi_B}$; $\bar{\mu}_R = \lambda_{\bar{w}} + \lambda_{\bar{q}} \Lambda_R \bar{\mathcal{S}}_\aleph$

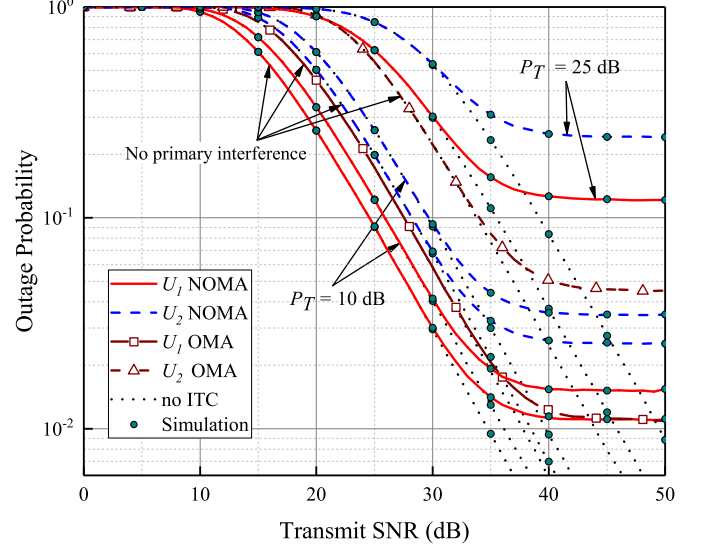


Fig. 2. The OP versus the transmit SNR for NOMA and OMA users with $I_{\text{ITC}} = 20$ dB, $\phi = 0$, $\vartheta = 0$ and $\zeta = 0$.

and $\bar{\xi}_R = \frac{\bar{\mathcal{O}}_\aleph}{\bar{\mathcal{S}}_\aleph} + \frac{\lambda_{\bar{q}}}{\lambda_{\bar{q}} \bar{\mathcal{S}}_\aleph}$. Notice that $\psi_B < \frac{\beta_B}{\bar{\mathcal{J}}_B}$, otherwise, $F_{\gamma_B}(\psi_B) \sim 1$. Finally, the exact OP of U_B can be derived by using (13) and (14).

IV. NUMERICAL RESULTS

This section discusses the numerical results and validates that all theoretical analyses precisely match with Monte-Carlo simulations. We assume two secondary NOMA users², i.e., U_1 and U_2 with the following system settings; the same transmit power levels at S and R , i.e., $P = P_S = P_R$; $\alpha_1 = \beta_1 = 0.8$; $\alpha_2 = \beta_2 = 0.2$; $\mathcal{R}_1 = 1$ bps; $\mathcal{R}_2 = 1.5$ bps; $d_{SR} = d_{R1} = d_{R2} = d$; $d_{SD} = d_{RD} = d_{TR} = d_{T1} = d_{T2} = 3d$, where d is assumed to be unity; $\tau = 3$.

Fig. 2 compares the OP of users operating on OMA and NOMA. For the sake of a fair comparison, the QoS demands of cooperative OMA is set as two-fold of that used for cooperative NOMA. To demonstrate the ITC impacts on the OP of SUs, we consider the asymptotic case, where D does not impose ITC, i.e., $I_{\text{ITC}} = \infty$. Fig. 2 shows that U_1 achieves a lower OP than U_2 since U_1 is assigned with a lower rate and

²In practice, it may not be feasible to consider many NOMA users due to the complexity and latency of SIC receivers, which increases non-linearly with the increase in the number of users [3]. In this work, SIC complexity especially becomes more significant because of the SIC error propagation.

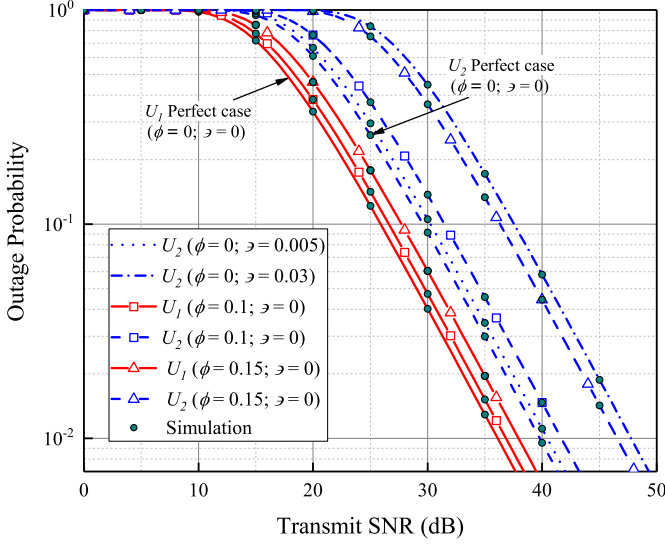


Fig. 3. The OP versus the transmit SNR for NOMA users with $P_T = 10$ dB, $I_{\text{ITC}} = \infty$ and $\zeta = 0$.

a higher PA factor. Also, notice that both NOMA users achieve a significantly lower OP than corresponding OMA modes. Additionally, we can observe that the ITC imposed at D , i.e., I_{ITC} , results in the saturation of OP curves. This implies that secondary transmitters cannot increase their transmission power above the ITC level in order not to cause harmful interference to D . A noteworthy observation is that an increase in primary interference level results in the outage performance deterioration of SUs. For example, at transmit SNR of 20 dB, U_1 obtains the OP of 0.09, 0.12 and 0.62 without primary interference, $P_T = 10$ dB and $P_T = 25$ dB, respectively.

Fig. 3 presents the impact of hardware and SIC imperfections on the OP of NOMA users considering perfect CSI ($\zeta = 0$). Here, we consider two imperfect SIC scenarios with $\varepsilon = 0.005$ and $\varepsilon = 0.03$. It is important to note that the higher level of SIC imperfection degrades the OP of NOMA users by causing full outage at intolerable imperfect SIC levels. For example, for the proposed system model with $\phi = 0$, the tolerable imperfect SIC level can be calculated from $\varepsilon < \frac{\alpha_2 - \phi^2}{\alpha_1 \psi_2}$ as $\varepsilon < 0.035$. Therefore, the plot shows that the imperfect SIC degrades the outage performance of U_2 . For instance, at 30 dB transmit SNR, U_2 obtains the OP of 0.105 and 0.45 when $\varepsilon = 0.005$ and $\varepsilon = 0.03$, respectively, while the OP for perfect SIC is 0.09. Additionally, we set two different HI levels as $\phi = 0.1$ and $\phi = 0.15$ to show the effect of HIs on the system performance. It is obvious that both NOMA users demonstrate better performance for the lower level of HI, as expected. A specific observation is that U_2 is more sensitive to the distortion noise than U_1 . For example, at 30 dB transmit SNR and $\phi = 0.15$, the OP of U_1 and U_2 degrades for 0.025 and 0.3, accordingly. Moreover, after comparing the outage performance of NOMA and OMA users, we note that, even in hardware limited scenario, the NOMA model still outperforms the OMA one. In addition, it is also noticed that the impact of HIs is more effective on the OMA user. For instance, when $\phi = 0.15$, the OP of NOMA user 2 degrades for the value of

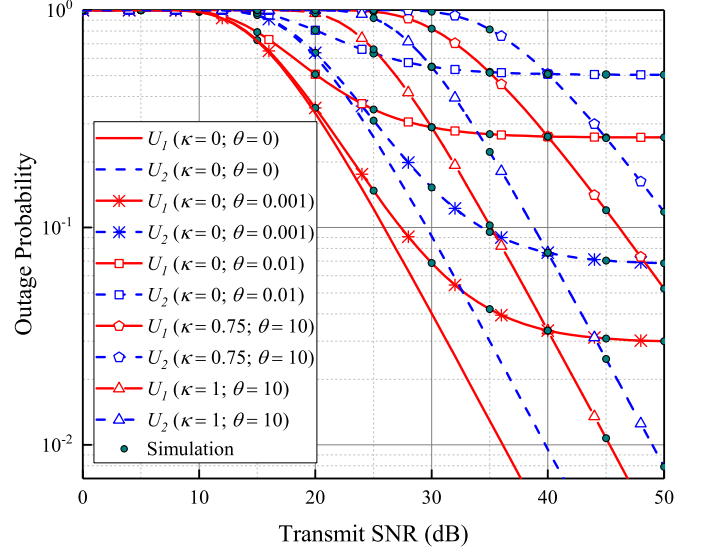


Fig. 4. The OP versus the transmit SNR for NOMA users with $P_T = 10$ dB, $I_{\text{ITC}} = \infty$ and $\phi = \varepsilon = 0$.

about 0.3, while the OP of OMA user 2 declares a full outage at all SNRs levels.

In Fig. 4, for the sake of figures clarity, we show the impact of the channel error variance on the outage performance of only U_1 considering NOMA and OMA models. We set the system parameters as $I_{\text{ITC}} = \infty$, $P_T = 10$ dB, $\phi = 0$ and $\varepsilon = 0$. It is observed from results that the NOMA user obtains better OP comparing with OMA one for all channel uncertainty scenarios. When $\kappa = 0$, the channel error variance becomes SNR-independent and increasing transmit SNR provides no advantage. However, the outage performance degrades by increasing θ . For instance, the OP of NOMA and OMA users saturate after 40 dB and 30 dB when $\theta = 0.001$ and $\theta = 0.01$, respectively. One observation is that, when θ is small, it does not cause considerable impact on the OP at lower SNR values. This reason is, when θ tends to zero, the channel estimation approaches to the perfect CSI. On the other hand, when $\theta = 0.1$, both NOMA and OMA users declare an outage at all SNR values, which means that the considered channel uncertainty is intolerable for these users. When $\kappa \neq 0$, OP saturation is not noticed as channel error model becomes SNR-dependent, and the increase of κ results in an improvement of the outage performance as the channel error is inversely proportional to the SNR. For example, when $\kappa = 1.5$ and $\theta = 10$, we can see that the impact of channel error decreases by increasing the SNR level and outage curves of both NOMA and OMA users approach the performance the perfect CSI at high SNRs.

V. CONCLUSION

This letter analyzed the performance of the downlink underlay CR-NOMA DF-based relaying network considering hardware, CSI, and SIC imperfections. Closed-form analytical expressions for the end-to-end OP of NOMA SUs were derived considering primary and secondary interference. Moreover, the proposed NOMA system model obtained better OP results

compared to the OMA one, which is considered as a benchmark model. Finally, the accurateness of the derived analytical expressions were verified by Monte Carlo simulations. In the future, the considered system model can be extended by considering the device-to-device mmWave communication.

APPENDIX A PROOF OF PROPOSITION 1

The term Δ in (9) can be derived as

$$\begin{aligned}\Delta &= \int_{z=0}^{\infty} f_Z(z) \int_{x=0}^{z\mathcal{K}_\Delta + \mathcal{M}_\Delta + \mathcal{L}} f_X(x) dx dz \int_{y=0}^{\Lambda_S} f_Y(y) dy \\ &= (1 - e^{-\lambda_y \Lambda_S}) \int_{z=0}^{\infty} \lambda_z e^{-\lambda_z z} \left(1 - e^{-\lambda_x (z\mathcal{K}_\Delta + \mathcal{M}_\Delta + \mathcal{L})}\right) dz \\ &= (1 - e^{-\lambda_y \Lambda_S}) \left(1 - \frac{\lambda_z e^{-\lambda_x (\mathcal{M}_\Delta + \mathcal{L})}}{\lambda_z + \lambda_x \mathcal{K}_\Delta}\right). \quad (\text{A.1})\end{aligned}$$

Then, the term Υ in (9) can be rewritten as follows

$$\Upsilon = \int_{z=0}^{\infty} f_Z(z) \underbrace{\int_{y=\Lambda_S}^{\infty} \int_{x=0}^{zy\mathcal{K}_\Upsilon + y\mathcal{M}_\Upsilon + \mathcal{L}} f_Y(y) f_X(x) dx dy}_{\Upsilon_1} dz, \quad (\text{A.2})$$

while the term Υ_1 in (A.2) can be calculated by

$$\begin{aligned}\Upsilon_1 &= \int_{y=\Lambda_S}^{\infty} \lambda_y e^{-\lambda_y y} \left(1 - e^{-\lambda_x (zy\mathcal{K}_\Upsilon + y\mathcal{M}_\Upsilon + \mathcal{L})}\right) dy \\ &= e^{-\lambda_y \Lambda_S} - \frac{\lambda_y e^{-\lambda_x \mathcal{L}} e^{-\Lambda_S (z\lambda_x \mathcal{K}_\Upsilon + \lambda_x \mathcal{M}_\Upsilon + \lambda_y)}}{z\lambda_x \mathcal{K}_\Upsilon + \lambda_x \mathcal{M}_\Upsilon + \lambda_y}. \quad (\text{A.3})\end{aligned}$$

Then, by inserting (A.3) into (A.2), we can rewrite Υ by

$$\begin{aligned}\Upsilon &= \int_{y=0}^{\infty} \lambda_z e^{-\lambda_z z} e^{-\lambda_y \Lambda_S} dz - \frac{\lambda_y \lambda_z e^{-\lambda_x \mathcal{L} - \lambda_x \Lambda_S \mathcal{M}_\Upsilon - \lambda_y \Lambda_S}}{\lambda_x \mathcal{K}_\Upsilon} \\ &\quad \times \int_{y=0}^{\infty} \frac{e^{-z(\lambda_z + \lambda_x \Lambda_S \mathcal{K}_\Upsilon)}}{z + \frac{\mathcal{M}_\Upsilon}{\mathcal{K}_\Upsilon} + \frac{\lambda_y}{\lambda_x \mathcal{K}_\Upsilon}}. \quad (\text{A.4})\end{aligned}$$

Now, by using [12, Eq. (3.352.4)], the term Υ can be derived in a closed-form as

$$\Upsilon = e^{-\lambda_y \Lambda_S} + \frac{\lambda_y \lambda_z e^{-\lambda_x (\mathcal{L} + \Lambda_S \mathcal{M}_\Upsilon) - \lambda_y \Lambda_S}}{\lambda_x \mathcal{K}_\Upsilon} e^{\mu_S \xi_S} \text{Ei}[-\mu_S \xi_S], \quad (\text{A.5})$$

where $\mu_S = \lambda_z + \lambda_x \Lambda_S \mathcal{K}_\Upsilon$; $\xi_S = \frac{\mathcal{M}_\Upsilon}{\mathcal{K}_\Upsilon} + \frac{\lambda_y}{\lambda_x \mathcal{K}_\Upsilon}$ and $\text{Ei}[\cdot]$ is the exponential integral function.

Finally, by inserting (A.1) and (A.5) into (9), the closed-form expression for the CDF of $\gamma_{R,j}$ can be written as in (10), where $\psi_j < \frac{\alpha_j}{A}$, otherwise, $F_{\gamma_{R,j}}(\psi_j) \sim 1$. ■

APPENDIX B PROOF OF PROPOSITION 2

The term Θ in (11) can be further extended as

$$\begin{aligned}\Theta &= \int_{w=0}^{\infty} f_W(w) \int_{q=0}^{w\mathcal{S}_\Theta + \mathcal{O}_\Theta + \mathcal{T}} f_Q(q) dq dw \underbrace{\int_{v=0}^{\Lambda_R} f_V(v) dv}_{\Theta_1} \\ &= \lambda_w \int_0^{\infty} e^{-\lambda_w w} dw - \lambda_w e^{-\lambda_q (\mathcal{O}_\Theta + \mathcal{T})} \int_0^{\infty} e^{-w(\lambda_w + \lambda_q \mathcal{S}_\Theta)} dw\end{aligned}$$

$$= (1 - e^{-\lambda_w \Lambda_R}) \left(1 - \frac{\lambda_w e^{-\lambda_q (\mathcal{O}_\Theta + \mathcal{T})}}{\lambda_w + \lambda_q \mathcal{S}_\Theta}\right). \quad (\text{B.1})$$

Further, we extend the term Φ in (11) as

$$\Phi = \int_{w=0}^{\infty} f_W(w) \underbrace{\int_{v=\Lambda_R}^{\infty} \int_{q=0}^{vw\mathcal{S}_\Phi + v\mathcal{O}_\Upsilon + \mathcal{L}} f_V(v) f_Q(q) dq dv}_{\Phi_1} dw, \quad (\text{B.2})$$

where Φ_1 can be derived as

$$\begin{aligned}\Phi_1 &= \lambda_v \int_{y=\Lambda_R}^{\infty} e^{-\lambda_v y} \left(1 - e^{-\lambda_q (wy\mathcal{S}_\Phi + v\mathcal{O}_\Upsilon + \mathcal{T})}\right) dy \\ &= e^{-\lambda_v \Lambda_R} - \frac{\lambda_v e^{-\lambda_q \mathcal{T}} e^{-\Lambda_R (w\lambda_q \mathcal{S}_\Phi + \lambda_q \mathcal{O}_\Upsilon + \lambda_v)}}{w\lambda_q \mathcal{S}_\Phi + \lambda_q \mathcal{O}_\Upsilon + \lambda_v}. \quad (\text{B.3})\end{aligned}$$

Then, by inserting (B.3) into (B.2), we can solve Φ as

$$\Phi = e^{-\lambda_v \Lambda_R} + \frac{e^{-\Lambda_R (\lambda_v + \lambda_q \mathcal{O}_\Upsilon) - \lambda_q \mathcal{T}}}{(\lambda_v \lambda_w)^{-1} \lambda_q \mathcal{S}_\Phi} (e^{\xi_R \mu_R}) \text{Ei}[-\mu_R \xi_R], \quad (\text{B.4})$$

where $\mu_R = \lambda_w + \lambda_q \Lambda_R \mathcal{S}_\Phi$ and $\xi_R = \frac{\mathcal{O}_\Upsilon}{\mathcal{S}_\Phi} + \frac{\lambda_v}{\lambda_q \mathcal{S}_\Phi}$. Finally, after inserting (B.1) and (B.4) into (11), the closed-form solution for the CDF of $\gamma_{b,j}$ can be found as in (12), where $\psi_j < \frac{\beta_b}{\mathcal{J}_b}$, otherwise, $F_{\gamma_{b,j}}(\psi_j) \sim 1$. ■

REFERENCES

- [1] "A guide to the internet of things." <https://www.intel.com/content/www/us/en/internet-of-things/infographics/guide-to-iot.html> Intel Corp., Accessed: 2020-04-07.
- [2] A. Celik and A. E. Kamal, "Green cooperative spectrum sensing and scheduling in heterogeneous cognitive radio networks," *IEEE Trans. Cognitive Commun. Netw.*, vol. 2, no. 3, pp. 238–248, 2016.
- [3] Z. Ding, M. Peng, and H. V. Poor, "Cooperative non-orthogonal multiple access in 5G systems," *IEEE Communications Letters*, vol. 19, pp. 1462–1465, Aug. 2015.
- [4] Y. Yu, Z. Yang, Y. Wu, J. A. Hussein, W. Jia, and Z. Dong, "Outage performance of NOMA in cooperative cognitive radio networks with SWIPT," *IEEE Access*, vol. 7, pp. 117308–117317, 2019.
- [5] X. Wang, M. Jia, Q. Guo, I. W. Ho, and F. C. Lau, "Full-duplex relaying cognitive radio network with cooperative nonorthogonal multiple access," *IEEE Systems Journal*, vol. 13, no. 4, pp. 3897–3908, 2019.
- [6] M. Jia et al., "Performance analysis of cooperative non-orthogonal multiple access based on spectrum sensing," *IEEE Transactions on Vehicular Technology*, vol. 68, no. 7, pp. 6855–6866, 2019.
- [7] V. Kumar, B. Cardiff, and M. F. Flanagan, "Fundamental limits of spectrum sharing for NOMA-based cooperative relaying under a peak interference constraint," *IEEE Transactions on Communications*, vol. 67, no. 12, pp. 8233–8246, 2019.
- [8] P. Aquilina and T. Ratnarajah, "Performance analysis of IA techniques in the MIMO IBC with imperfect CSI," *IEEE Transactions on Communications*, vol. 63, no. 4, pp. 1259–1270, 2015.
- [9] S. Arzykulov, G. Naurzybayev, T. A. Tsiftsis, B. Maham, and M. Abdallah, "On the outage of underlay CR-NOMA networks with detect-and-forward relaying," *IEEE Transactions on Cognitive Communications and Networking*, vol. 5, pp. 795–804, Sep. 2019.
- [10] Z. Ding et al., "Relay selection for cooperative NOMA," *IEEE Wireless Communications Letters*, vol. 5, no. 4, pp. 416–419, 2016.
- [11] S. Sesia, I. Toufik, and M. Baker, *LTE - The UMTS Long Term Evolution: From Theory to Practice*. Wiley Publishing, USA, 2nd ed., 2011.
- [12] I. S. Gradshteyn and I. M. Ryzhik, *Table of integrals, series, and products*. Elsevier/Academic Press, Amsterdam, 7th ed., 2007.